Printing 3D Gel Polymer Electrolyte in Lithium-Ion Microbattery Using Stereolithography

Journal of The Electrochemical Society, **164** (9) A1852-A1857 (2017)
0013-4651/2017/164(9)/A1852/6/$37.00 © The Electrochemical Society

Printing 3D Gel Polymer Electrolyte in Lithium-Ion Microbattery Using Stereolithography

Qiming Chen, Rong Xu, Zitao He, Kejie Zhao,* and Liang Pan[z]

School of Mechanical Engineering, Birck Nanotechnology Center, Purdue University, West Lafayette, Indiana 47906, USA

Here we demonstrate the use of projection stereo-micro-lithography as a low-cost and high-throughput method to fabricate three dimensional (3D) microbattery. An Ultraviolet (UV)-curable Poly (ethylene glycol) (PEG)-base gel polymer electrolyte (GPE) is first created. The GPE is then used as a resin for micro-stereolithography in order to build a 3D architecture of battery's electrolyte. Active materials, $LiFePO_4$ (LFP) and $Li_4Ti_5O_{12}$ (LTO), are mixed with carbon black and the GPE resin, which is then flown into the 3D structure. Aluminum (Al) foil is cut and inserted as a current collector. The GPE is characterized and the microbattery is performed a cycling test. Results show a feasibility of microbattery fabrication using projection micro-stereolithography.

Manuscript submitted January 30, 2017; revised manuscript received June 21, 2017. Published June 30, 2017. This was Paper 1339 presented at the New Orleans, Louisiana, Meeting of the Society, May 28–June 1, 2017.

MICRO-scale device has gained a lot of attentions since the development of micro- and nano-technologies, which drives the demand for micro-scale energy storage devices. Among all the rechargeable energy storage systems, lithium-ion battery exhibits the highest energy density. Therefore, researchers have shown great interest for the development of high performance lithium-ion microbatteries. The planar thin film microbattery was first introduced by Oak Ridge National Laboratory[1] where the battery capacity is determined by the battery footprint. In order to fully utilize the limited area, 3D microbattery was developed as an alternative technology for small scale energy storage,[2–10] where the ultimate goal is to obtain a high surface area substrate coated with thin layers of cathode, electrolyte and anode materials to enhance the energy density per footprint area. Also, the 3D architecture with a larger active surface area can facilitate the ion transfer between electrolyte and active material, thus achieving fast energy storage and release. Therefore, among the many concepts of the term "3D battery", one of them denotes the "cells comprising anodes and cathodes which have active surface areas exposed in three dimensions".[11]

The critical step to fabricate 3D microbattery is to pattern the 3D microscale geometry. C. Wang[12] and H. Min[13] fabricated microrods with pyrolized photoresist through conventional photolithography. K. Sun[14] built the microelectrode array layer by layer using the 3D filamentary printing and achieved a high aspect ratio battery architecture. H. Ning[15] combined 3D holography with 2D photolithography to define the manifolds for microbattery electrodes. G. Oltean[16] obtained aluminum nanorods as negative electrode and LFP-coated carbon foam as positive electrode. C. Liu[17] built the all-in-one nanopore battery array using anodic aluminum oxide (AAO) template and atomic layer deposition (ALD). However, these 3D electrodes are all patterned through multiple steps which leads to higher material and time consumptions. Moreover, recent developments in additive manufacturing have advanced the previous 3D printing technologies from the industrial prototyping processes into affordable tools for both research studies and niche manufacturing. This also leads to some new applications for fully-printed electronics that discourages the use of conventional battery assembly and allows limited footprint area for the battery unit. In this work, we demonstrated the use of projection micro-stereolithography, one of the fastest microscale 3D printing technologies, to directly pattern a 3D microbattery in an additive process using photocurable poly(ethylene oxide) (PEO)-based resin. With the high resolution of our system and the capability to change projection patterns, microbattery with smaller footprint can be fabricated so that parallel manufacturing of multiple microbatteries on one substrate can be achieved. This current process can grow 3D microstructures at a speed of ~10 μm/s over a 1-cm^2 footprint. The fabrication process doesn't use sacrificial or evaporative materials or generate additional chemical wastes. Moreover, compared with other methods of fabricating 3D microbattery, the projection micro-stereolithography method is essentially a parallel additive process which can produce sophisticated 3D microstructures at economical material utilization, low cost and high throughput.

The PEO-based solid polymer electrolyte material has proven to be ionic conductive for lithium ion.[18] The PEO material has an ionic conductivity of 10^{-7}-10^{-8} S cm^{-1} in the room temperature due to the restrict segmental motion of PEO chains, which limits its commercial use in lithium-ion batteries.[19] There are several ways to improve the conductivity, such as adding plasticizer to reduce the crystalline region[20,21] and adding organic solvents to form a gel polymer electrolyte.[22,23] The PEO-based gel polymer electrolyte can have significantly high ionic conductivity. R. He[24] applied cross-linked poly(ethylene glycol) diacrylate (PEGDA), plasticized by Succinonitrile (SCN), to form a solvent-free polymer electrolyte, which shows a promising ambient temperature ion conductivity (1.4×10^{-3} $S \cdot cm^{-1}$). S. Kim[25,26] used a tri-functional monomer, mixed with lithium salt and organic solvents and then photocured to form gel electrolyte, with conductivity above 1.0×10^{-3} $S \cdot cm^{-1}$. Y. Kang[27] mixed the poly(ethylene glycol) dimethylether (PEGDMA) with liquid electrolyte and formed a gel electrolyte (plasticized by its carbonate solvents) with a conductivity up to 5.1×10^{-4} $S \cdot cm^{-1}$ at 30°C. Applying the gel electrolyte: 1) can provide the shape flexibility of battery and make a 3D battery with larger surface area between electrolyte and active material, thus a higher energy density per footprint area; 2) may avoid the requirement for hermetical sealing, which is in the case of liquid electrolyte; 3) promises a relatively higher ionic conductivity than solid polymer electrolyte.

Experimental

Materials.—The UV-curable resin for micro-stereolithography is a mixture of 97% (in weight) PEGDA (Sigma Aldrich, Mn = 575 g/mol), 1% of phenylbis(2,4,6-trimethyl-benzoyl)phosphine oxide (Sigma Aldrich) as a photo-initiator and 2% of photoabsorber Sudan I (Sigma Aldrich). The GPE resin composes of 20% (in volume) of UV-curable resin and 80% 1 M $LiClO_4$ (EC/PC = 1/1 in volume) liquid electrolyte. The low molecular weight and high boiling point PC and EC can act as plasticizer to reduce the crystallization of polymer, which will increase the ionic conductivity but meanwhile make the electrolyte membrane brittle. $LiClO_4$ is used as the lithium salt because it is less sensitive to the atmospheric moisture.[28]

The electrode slurries used in this work are home made in gel forms. The electrode slurries are mixtures of 1 g GPE resin, 0.16 g Super P carbon black and 0.7 g active materials. The lithium iron phosphate (LFP or $LiFePO_4$) and lithium titanate (LTO or $Li_4Ti_5O_{12}$) are used as active materials for cathode and anode respectively. These

*Electrochemical Society Member.
[z]E-mail: liangpan@purdue.edu

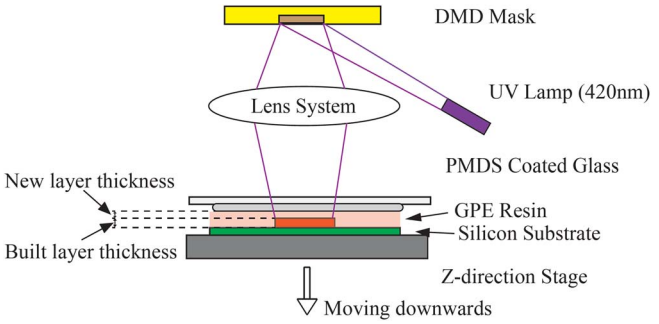

Figure 1. Configuration of 3D micro-stereolithography platform.

materials were purchased from MTI corporation. After agitating on vortex mixer for 5 minutes, the slurries are then flown into the 3D architecture. Since the couple of LFP/LTO has a redox potential within the stable window of aluminum, aluminum foils can be used as current collectors for both electrodes.[29]

Micro-stereolithography.—Micro-stereolithography, also known as μSLA, is a form of additive manufacturing that fabricates structure layer by layer using photopolymerization. The μSLA system we built has the ability to fabricate microstructure with a resolution better than 10 μm, determined by the original pixel size of the digital micromirror device (DMD) and the demagnification factor associated with the optical projection system.[30] Therefore, by curing the liquid resin, the system can fabricate patterns in microscale. The resin is a photopolymer and can be cured by an UV lamp in seconds.

When fabricating a microstructure, the UV light penetrates the photopolymer resin at a microscale depth well-controlled by the concentration of the photo-absorber.[31] The resin contains photoinitiator which will generate free radicals after absorbing the UV light. The radical later reacts with double bonds in low-molecular-weight polymer, causing chain growth or polymerization. Light penetration depth, therefore, determines the curing depth and also the layer thickness. The curing depth can be changed by adding photoabsorber into the resin. Through changing the composition of the resin, the printed 3D structure will have different mechanical properties and layer thicknesses.[31]

The μSLA system we built composes of three modules: 1) the motorized recoating platform, 2) optical projection systems and 3) digital micromirror device (DMD). The motorized recoating platform has a unidirectional resolution of 50 nm. During fabrication, the PDMS coated glass is fixed at the position of projected UV image and the printed part is carried by the motorized recoating platform. After each curing step, the motorized recoating platform moves downwards which creates rooms to let fresh resin to flow in between the printed part and the PDMS glass. As shown in Fig. 1, fresh resin layer is shown between top glass window and a part built onto a silicon substrate. The top glass window is spin-coated with polydimethylsiloxane (PDMS) to be hydrophobic, which facilitates the release of newly-built layer after each curing step. The projection pattern irradiated on the top of cover glass is predefined by the DMD mask, with a maximum footprint of 12.6 mm by 7.1 mm. This maximum footprint area can be increased by adjusting the magnification of the projection optics at a trade-off of resolution. The silicon substrate is treated by 3-(Trimethoxysilyl)propyl methacrylate(TMSPMA) as surfactant to ensure the attachment during the printing process.[32] After the fabrication, the sample will be rinsed with isopropyl alcohol for removing the extra uncured resin. The sample is then dried by clean dry air before microbattery assembly.

3D GPE is fabricated on this stereolithography platform. We designed the 3D battery structure first in CAD. The model is then sliced into 100 layers and each of them has a thickness of 30 μm. The layers generated are used as the projection pattern for stereolithography. For each curing step, the motorized platform moves downwards for 30 μm to create a new layer. UV light will irradiate on the resin for 13 seconds in order to fully cure the layer. After that, the platform moves downwards again to prepare for the next curing.

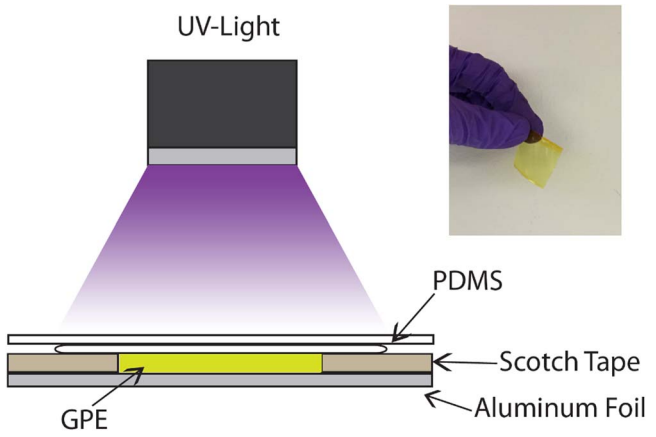

Figure 2. GPE membrane fabricated using scotch tape to control thickness.

GPE material characterization.—GPE membrane is first fabricated into thin film with controlled thickness for electrochemical property testing. As shown in Fig. 2, the GPE resin is first dropped onto an Aluminum foil. In order to control the thickness of the membrane, the resin is sandwiched between the PDMS-coated glass and an aluminum foil with a native aluminum oxide layer.[33] Two pieces of scotch tape of 62.5 μm thick are used as spacers as illustrated in Fig. 2. After spreading the resin with a uniform thickness, the resin is photocured into GPE membrane. After removing the PDMS-coated glass, the GPE membrane is later peeled off from the aluminum foil for further tests.

The gel LFP and LTO electrodes are manufactured by conventional slurry casting method on aluminum foil. The two electrodes are wetted by liquid electrolyte and then put together with GPE membrane to form a battery prototype as shown in Fig. 3. A potentiostatic charging at 4.0 V is conducted on the battery prototype. The battery is able to discharge at 1.6 V to power a red LED for minutes. Further cycling proves the rechargeability of the GPE membrane. The result proves the feasibility of the GPE membrane in lithium-ion battery application. There is a substantial voltage difference for charge and discharge cycles which was mainly caused by the ionic resistance of GPE membrane and the internal resistances due to small foot print area and poor components contact.

Further test has been performed on Arbin BT-2000 with a GPE half-cell. The half-cell is assembled in glove box with commercial LFP as cathode and lithium metal as anode. The electrodes are wetted by $LiClO_4$(EC+PC) electrolyte. GPE membrane is cut into a circular shape and put together with the electrodes. The standard C/20 and C/5 cycling have been performed which validate GPE as a separator in a lithium-ion battery (see details in Result and Discussion). Also, the electrochemical activities of individual electrode materials are

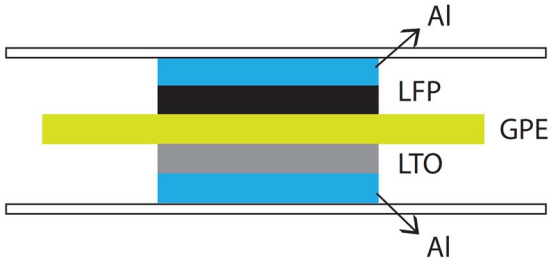

Figure 3. Coin cell structure battery prototype assembly and testing.

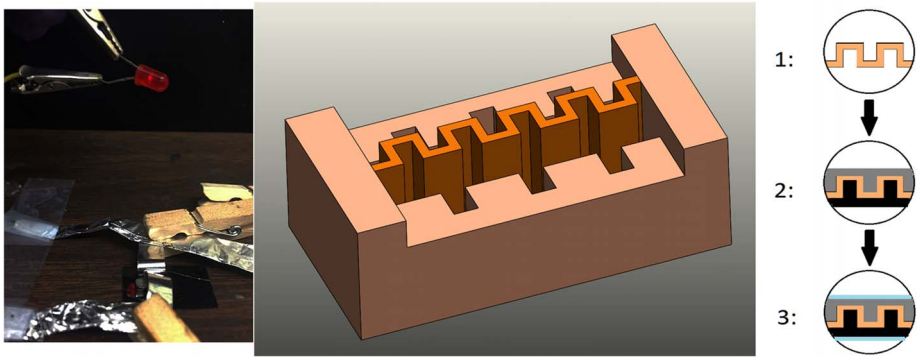

Figure 4. Left: 3D structure for GPE; Right: assembly process for microbattery in top view. (1.GPE zigzag center membrane; 2.fill-in of active materials and GPE resin mixture; 3.Al current collector insertion)

confirmed in cyclic voltammetry using the electrode/GPE/lithium half cell configurations.

Electrode mixtures .—The conventional slurry casting method cannot be easily applied to 3D electrode fabrication due to the lack of geometry flexibility. To construct a 3D microbattery with conformal contact between the micro-structured GPE and electrode materials, we made a gel-form electrode materials as described in Materials section, consist of a mixture of GPE resin, carbon black and active materials. The solid contents in the mixture ensure the electrode's electrical conductivity, while the liquid resin can increase the ionic conductivity in electrodes and allow the gel-form electrode materials to implant into the printed 3D micro-structured GPE. It is worth to note that the weight ratio of solid content in the electrodes is high enough (40% or more) in order to maintain a good electronic and ionic conductivity and enable normal faradaic reaction. The active materials (LTO and LFP) are microparticles with a diameter of tens of micrometer. It is reported[34] that a good dispersion state of LFP particles and carbon black additives can be achieved in the GPE resin and solid particles mixture, and it results in the formation of electronic networks in electrode. Also, the liquid electrolyte can provide conductive pathways for lithium ions.

The material has been characterized in a coin cell assembled in glove box. Both cathode (LFP) and anode (LTO) mixtures are loaded on aluminum current collector. GPE is cured and punched into a circular shape, which has a diameter slightly larger than aluminum current collectors. The coin cell is then performed cycle tested on Arbin BT-2000.

Microbattery assembly and testing.—Although fabricating complicated 3D geometry are possible by micro-stereolithography, our proof-of-concept 3D-microbattery contains features facilitate laboratory handling and testing. As shown in Fig. 4, the micro-structured GPE has an overall footprint area of 7.6 mm by 3.8 mm, and a height of 3.0 mm. Two trenches are to be filled by the current collectors and the electrode materials. The three cuts on the sides of both trenches provide a channel for electrode mixtures to implant into later. The center membrane acts as the battery's gel electrolyte and is designed into a zigzag shape in order to increase the contact area between electrode and electrolyte. The center membrane is higher than the sides for experimental handling purpose which prevents the electrode mixture from overflowing to the other side. In addition, we directly print a support structure using GPE to surround the functional part of 3D microbattery.

As seen in Fig. 5, the thickness of the GPE membrane is 200 μm and contains sub-micron scale channeling formed during the photopolymerization process. This self-assembled sub-micron scale channels can help to further enhance the ion transport by reducing

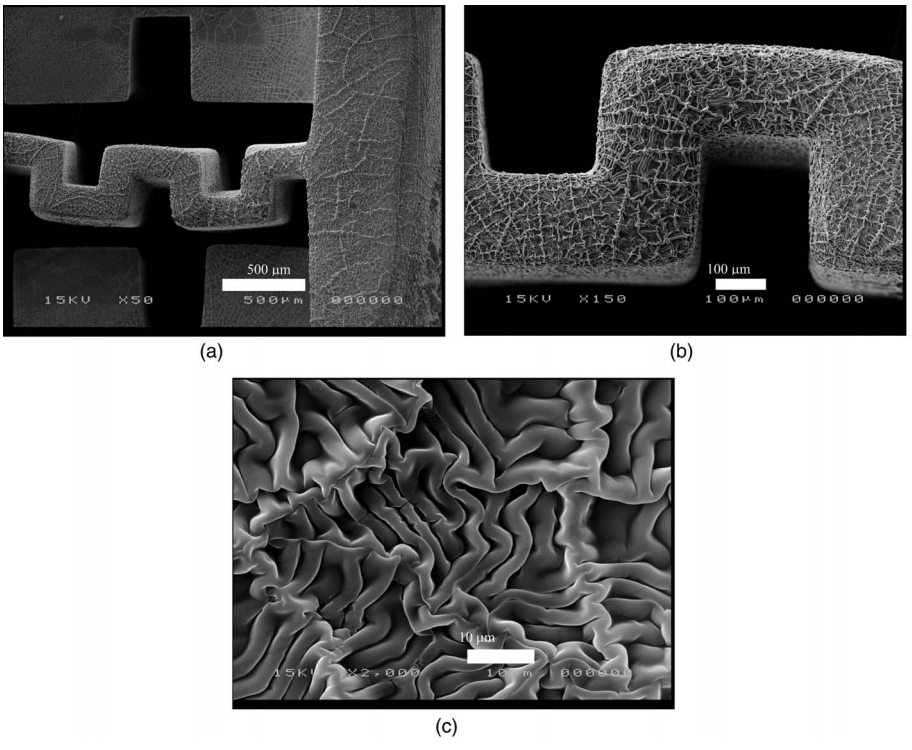

Figure 5. The SEM pictures for GPE 3D structure: (a) Top view of GPE; (b) top view of the zigzag structure; (c) PEG polymer matrix.

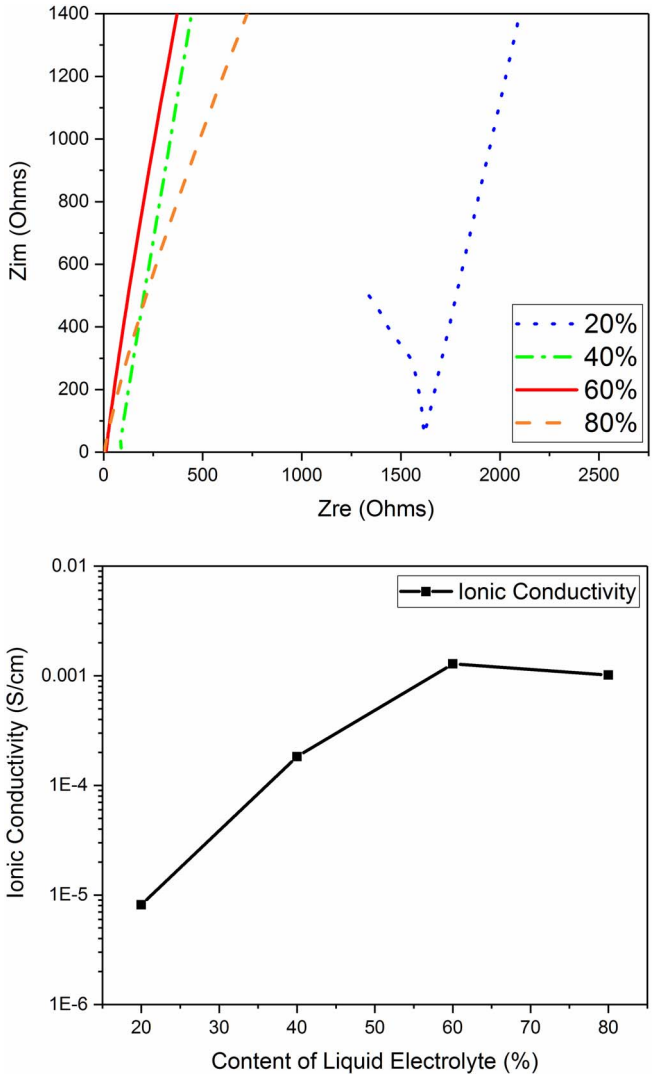

Figure 6. Ionic conductivity as a function of volume percentage of liquid electrolyte (lower layer, B) and Nyquist plots (upper layer, A) of the SS/GPE/SS symmetrical cell. Electrode area: 1.77 cm^2 (I.80% Electrolyte, $R_l = 15.0\ \Omega$, t = 270 μm; II.60% Electrolyte, $R_l = 11.0\ \Omega$, t = 250 μm; III.40% Electrolyte, $R_l = 80.2\ \Omega$, 260 μm; IV.20% Electrolyte, $R_l = 1.6\ k\Omega$, 230 μm.)

interfacial scattering, similar to the porous structures in conventional battery separators.[35]

The LFP mixture appears to be black while the LTO one is more gray. Their colors allow us to visually confirm that the electrode materials are properly filled into the textures of zigzag geometry. This is followed by inserting the aluminum current collector into the side trenches.

Result and Discussion

Ionic conductivity .—The Electrochemical Impedance Spectrum (EIS) is performed for analysis of GPE's lithium ion conductivity. GPE membranes with different electrolyte fractions have been fabricated for testing. During testing, the GPE membranes are inserted between two piece of stainless steel and inserted to a test cell. Its conductivity can be calculated as $\sigma = R_l^{-1} A^{-1}t$, where t is the thickness, R_l is the intercept with real axis from EIS measurement, and A is the surface area of stainless steel. The EIS result is shown in Fig. 6. The ionic conductivity of UV-cured GPE membrane strongly depends on the volume percentages of liquid electrolyte in GPE resin. Compared with the 20% volume percentages, the 80% volume percentages of liquid electrolyte in GPE resin can enhance the ionic conductivity to 4.8×10^{-3} S/cm at room temperature, which is close to the liquid electrolyte.

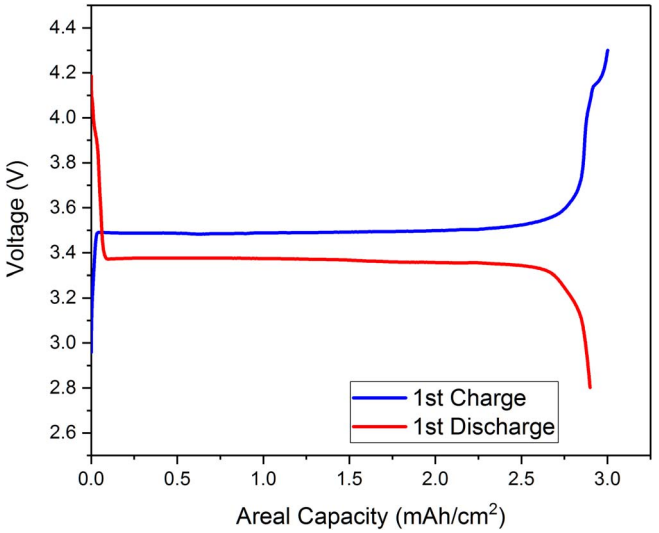

Figure 7. Cycle test for LFP/GPE/Li coin cell at charging rate of C/20.

GPE are hybrid systems consisting in a polymer matrix, trapping, by physical and chemical bonds, a liquid content.[36] Therefore, the photo-polymerized PEGDA network, mixed with the liquid electrolyte, can form a stable gel electrolyte without losing the organic solvent as well as improved mechanical stability.[37] Also, its ionic conductivity will be increased since lithium salt is added into the PEG, and the solvated lithium salt will facilitate the transportation of Li^+. Moreover, the lithium ion transport in GPE is mainly contributed to the amorphous region, as a result of adding the organic solvents as plasticizer. Therefore, adding more liquid electrolyte will increase the mobility of polymer chains due to an increase amount of amorphous region.

GPE characterization.—Voltage profile of the GPE half-cell's first cycle is presented in Fig. 7. A slow charging current (C/20) is applied on the half-cell battery. Due to the high ionic conductivity of GPE, the result shows a clear charging plateau around 3.5 V (Li/Li^+) and discharge plateau around 3.4 V, which is close to the theoretical charge/discharge plateau of LFP. The coulombs efficiency is of 97.7%. This represents a good electrochemical stability between the active material and the GPE.

Further cycling test is continued with a higher charging current (C/5) as shown in Fig. 8. The capacity has a slightly decrease in the second and third cycle, and drops suddenly to near 40% in the fourth cycle. The half-cell exhibits catastrophic failure at the 10^{th} cycle. This possibly results from the dendrite growth in lithium anode during the cycle, which causes short circuit between electrodes. Several papers[38,39] have reported the similar cycling failures and recommended remedies. It is reported that by adding SiO_2 to the polymer electrolyte, lithium dendrite can be mechanically surpassed and good capacity retention can be achieved.[40] Also, in other papers, a similar PEG-based recipe is applied and cured on a separator membrane, which increase the GPE's mechanical strength. The result from this separator-based GPE research shows a good cycle performance in full cell test.[41,42] They have a very similar recipe with ours, but in comparison to our work, their membrane is more robust with support of separator, and thus has a better electrochemical performance.

Electrode mixture characterization.—The electrode mixture, together with the GPE is tested in coin cell assembled in glove box. The charging current is set to be 50 μA which is a discharging current 5 μA. The result in Fig. 9 shows a successful 5 cycles. However, no

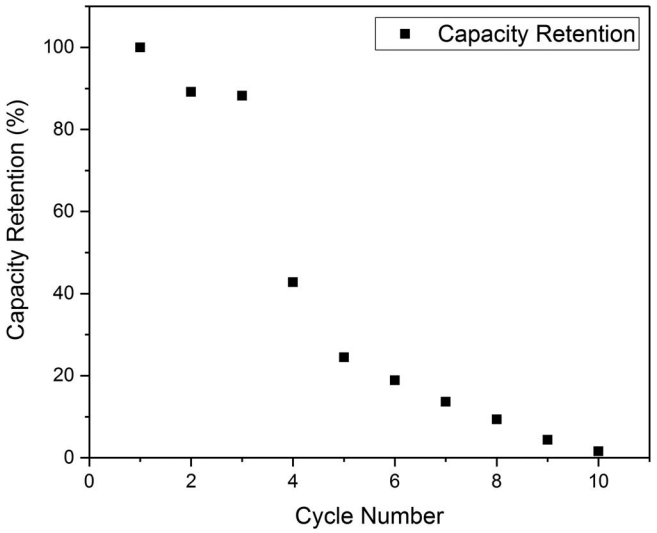

Figure 8. Capacity retention for LFP/GPE/Li half-cell at charging rate of C/5.

apparent charging plateau is observed and the discharging voltage is apparently lower than the normal LFP/LTO full-cell battery. These are possibly because of the large internal resistance caused by the poor contact between electrode and current collector due to a large amount of liquid content in electrode material. Therefore, it results in a low coulombs efficiency and a degradation of capacity. Also, a gassing problem is found in the anode side during charging. This is because of the reaction between LTO and the liquid electrolyte, generating gaseous products.[43] Although further improvements are needed on these electrode mixtures, they allow us to perform proof-of-concept tests to demonstrate the possibility of printing a 3D microbattery using micro-stereolithography.

Microbattery test.—The result shows a feasibility of manufacturing full-cell battery using 3D printed GPE. Because the 3D microbatteries cannot fit into the standard battery testers, we performed tested by ampere meters and voltage meters. The microbattery is charged at 4.2 V and discharged at 1.5 V potentiostatically. The current has been measured during the process. During charging process, the current varies from 30 μA to 90 μA. While during discharging, the current is between 2 μA to 4 μA. The specific areal discharging capacity is calculated to be 1.4 μAh/cm^2. The battery can successfully be operated for 2 cycles as shown in Fig. 10.

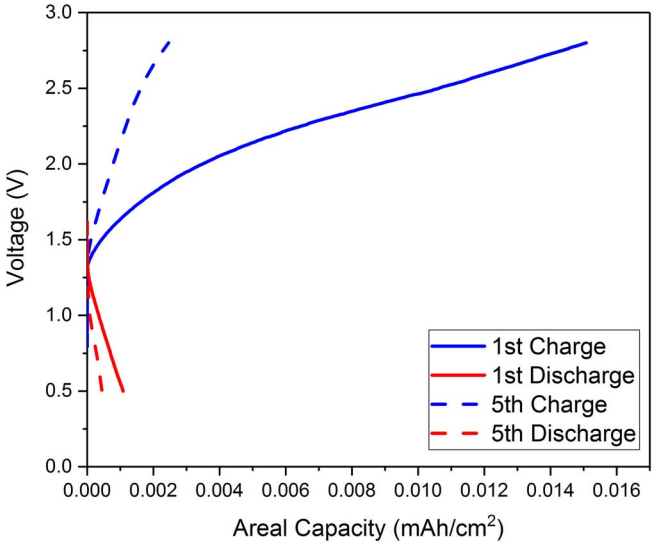

Figure 9. Cycle test for electrode mixture with GPE.

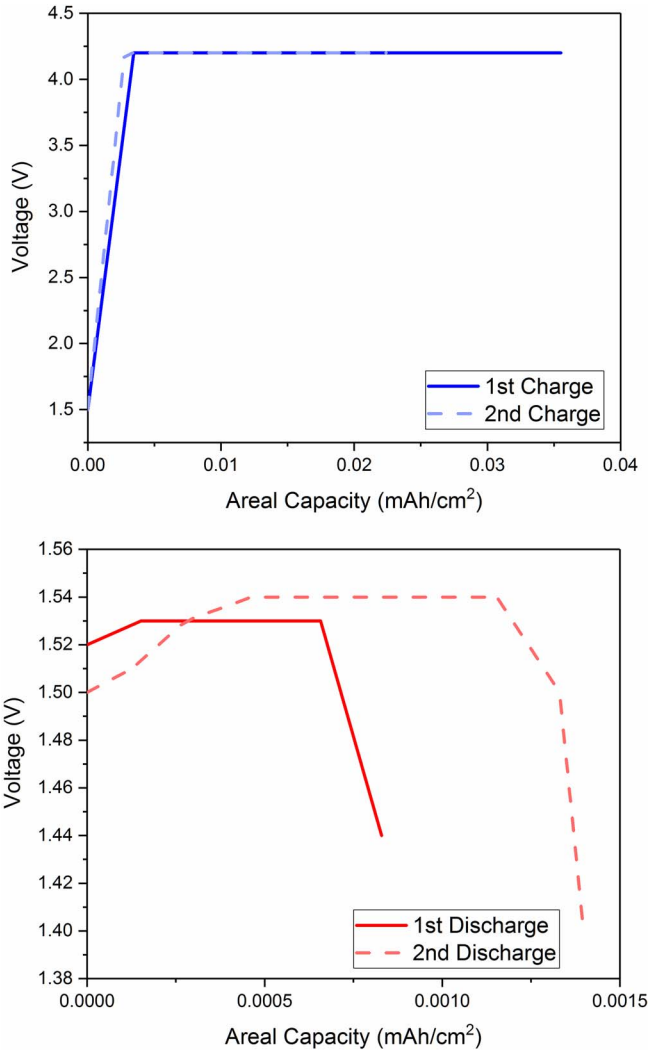

Figure 10. Microbattery cycling test using potentiostatic charging (upper layer) and discharging (lower layer).

The microbattery failed at the 3rd cycle, which does not match the result from electrode mixture characterization. This is possibly due to the reaction between air or moisture and the battery's components. When the electrode mixture characterization is performed in argon-filled coin cell environment, the 5 cycles are successfully conducted.

Conclusions

Micro-stereolithography has been successfully applied in fabrication of lithium ion microbattery. A UV-cured PEO-based GPE membrane is synthesized and characterized. The result shows it a high ionic conductivity membrane in room temperature and a potential in replacement of the lithium-ion battery's separator. 3D GPE architecture is then built by the stereolithography, which is followed by the microbattery assembly. The result shows a successful operation of microbattery for 2 cycles under potentiostatic charging condition, with a measured capacity of 1.4 μAh/cm^2. The stereolithgraphy method offers a low-cost and high-yield method for manufacturing 3D microbattery. It can easily create different 3D geometries, which facilitates the microbattery's design and prototype process. Despite of process advantages of micro-stereolithography for manufacturing 3D microbattery, the current process is still significantly slower and more expensive than mass produced conventional 2D batteries of the same

capacity. Future work of this topic should be focused on increasing the cycle performance for the GPE membrane as well as for microbattery. 3D solid electrode needs to be applied in order to reduce the microbattery's internal resistance.

References

1. J. B. Bates, N. J. Dudney, D. C. Lubben, G. R. Gruzalski, B. S. Kwak, X. Yu, and R. A. Zuhr, *Journal of Power Sources*, **54**(1), 58 (1995).
2. S. Ferrari, M. Loveridge, S. D. Beattie, M. Jahn, R. J. Dashwood, and R. Bhagat, *Journal of Power Sources*, **286**, 25 (2015).
3. J. F. M. Oudenhoven, L. Baggetto, and P. H. L. Notten, *Advanced Energy Materials*, **1**(1), 10 (2011).
4. Y. Wang, B. Liu, Q. Li, S. Cartmell, S. Ferrara, Z. D. Deng, and J. Xiao, *Journal of Power Sources*, **286**, 330 (2015).
5. M. Roberts, P. Johns, J. Owen, D. Brandell, K. Edstrom, G. El Enany, C. Guery, D. Golodnitsky, M. Lacey, C. Lecoeur, H. Mazor, E. Peled, E. Perre, M. M. Shaijumon, P. Simon, and P. -L. Taberna, *Journal of Materials Chemistry*, **21**(27), 9876 (2011).
6. T. S. Arthur, D. J. Bates, N. Cirigliano, D. C. Johnson, P. Malati, J. M. Mosby, E. Perre, M. T. Rawls, A. L. Prieto, and B. Dunn, *Mrs Bull*, **36**(07), 523 (2011).
7. J. W. Long, B. Dunn, D. R. Rolison, and H. S. White, *Chemical Reviews*, **104**(10), 4463 (2004).
8. M. Roberts, P. Johns, J. Owen, D. Brandell, K. Edstrom, G. El Enany, C. Guery, D. Golodnitsky, M. Lacey, C. Lecoeur, H. Mazor, E. Peled, E. Perre, M. M. Shaijumon, P. Simon, and P. -L. Taberna, *Journal of Materials Chemistry*, **21**(27), 9876 (2011).
9. M. Valvo, M. Roberts, G. Oltean, B. Sun, D. Rehnlund, D. Brandell, L. Nyholm, T. Gustafsson, and K. Edström, *Journal of Materials Chemistry A*, **1**(32), 9281 (2013).
10. S. R. Gowda, A. L. Reddy, X. Zhan, H. R. Jafry, and P. M. Ajayan, *Nano letters*, **12**(3), 1198 (2012).
11. R. W. Hart, H. S. White, B. Dunn, and D. R. Rolison, *Electrochemistry Communications*, **5**(2), 120 (2003).
12. C. Wang, L. Taherabadi, G. Jia, M. Madou, Y. Yeh, and B. Dunn, *Electrochemical and Solid-State Letters*, **7**(11), A435 (2004).
13. H. -S. Min, B. Y. Park, L. Taherabadi, C. Wang, Y. Yeh, R. Zaouk, M. J. Madou, and B. Dunn, *Journal of Power Sources*, **178**(2), 795 (2008).
14. K. Sun, T. S. Wei, B. Y. Ahn, J. Y. Seo, S. J. Dillon, and J. A. Lewis, *Advanced materials*, **25**(33), 4539 (2013).
15. H. Ning, J. H. Pikul, R. Zhang, X. Li, S. Xu, J. Wang, J. A. Rogers, W. P. King, and P. V. Braun, *Proceedings of the National Academy of Sciences of the United States of America*, **112**(21), 6573 (2015).
16. G. Oltean, H. Desta Asfaw, L. Nyholm, and K. Edstrom, *ECS Electrochemistry Letters*, **3**(6), A54 (2014).
17. C. Liu, E. I. Gillette, X. Chen, A. J. Pearse, A. C. Kozen, M. A. Schroeder, K. E. Gregorczyk, S. B. Lee, and G. W. Rubloff, *Nature nanotechnology*, **9**(12), 1031 (2014).
18. D. Fenton, J. Parker, and P. Wright, *polymer*, **14**(11), 589 (1973).
19. J. W. Fergus, *Journal of Power Sources*, **195**(15), 4554 (2010).
20. Y. Ito, K. Kanehori, K. Miyauchi, and T. Kudo, *Journal of Materials Science*, **22**(5), 1845 (1987).
21. I. E. Kelly, J. R. Owen, and B. C. H. Steele, *Journal of Power Sources*, **14**(1-3), 13 (1985).
22. J. M. Tarascon, A. S. Gozdz, C. Schmutz, F. Shokoohi, and P. C. Warren, *Solid State Ionics*, **86–88**, 49 (1996).
23. Z. Ren, K. Sun, Y. Liu, X. Zhou, N. Zhang, and X. Zhu, *Solid State Ionics*, **180**(9-10), 693 (2009).
24. R. He, M. Echeverri, D. Ward, Y. Zhu, and T. Kyu, *Journal of Membrane Science*, **498**, 208 (2016).
25. S.-H. Kim, (2015).
26. E. H. Kil, K. H. Choi, H. J. Ha, S. Xu, J. A. Rogers, M. R. Kim, Y. G. Lee, K. M. Kim, K. Y. Cho, and S. Y. Lee, *Advanced materials*, **25**(10), 1395 (2013).
27. Y. Kang, H. J. Kim, E. Kim, B. Oh, and J. H. Cho, *Journal of Power Sources*, **92**(1-2), 255 (2001).
28. K. Xu, *Chemical Reviews*, **104**(10), 4303 (2004).
29. N. Li, Z. Chen, W. Ren, F. Li, and H. M. Cheng, *Proceedings of the National Academy of Sciences of the United States of America*, **109**(43), 17360 (2012).
30. R. Wasielewski, C. Jin, P. Liang, and J. A. Weibel, 134 (2016).
31. C. Sun, N. Fang, D. M. Wu, and X. Zhang, *Sensors and Actuators A: Physical*, **121**(1), 113 (2005).
32. H. Xu, M. M. Ferreira, and S. C. Heilshorn, *Lab on a chip*, **14**(12), 2047 (2014).
33. M. Rahimi, P. Fojan, L. Gurevich, and A. Afshari, *Applied Surface Science*, **296**, 124 (2014).
34. S. H. Kim, K. H. Choi, S. J. Cho, S. Choi, S. Park, and S. Y. Lee, *Nano letters*, **15**(8), 5168 (2015).
35. D. T. Wong, S. A. Mullin, V. S. Battaglia, and N. P. Balsara, *Journal of Membrane Science*, **394–395**, 175 (2012).
36. J. Hassoun and B. Scrosati, *Journal of The Electrochemical Society*, **162**(14), A2582 (2015).
37. Y. Kang, K. Cheong, K.-A. Noh, C. Lee, and D.-Y. Seung, *Journal of Power Sources*, **119–121**, 432 (2003).
38. L. Porcarelli, C. Gerbaldi, F. Bella, and J. R. Nair, *Scientific reports*, **6**, 19892 (2016).
39. R. Khurana, J. L. Schaefer, L. A. Archer, and G. W. Coates, *Journal of the American Chemical Society*, **136**(20), 7395 (2014).
40. W.-K. Shin, S.-M. Park, Y.-S. Lee, and D.-W. Kim, *Journal of The Electrochemical Society*, **162**(14), A2628 (2015).
41. W. Kim, J.-J. Cho, Y. Kang, and D.-W. Kim, *Journal of Power Sources*, **178**(2), 837 (2008).
42. Y. Kang, W. Lee, D. Hack Suh, and C. Lee, *Journal of Power Sources*, **119–121**, 448 (2003).
43. M. He, E. Castel, A. Laumann, G. Nuspl, P. Novak, and E. J. Berg, *Journal of the Electrochemical Society*, **162**(6), A870 (2015).

Journal of The Electrochemical Society, **164** (9) X18-X18 (2017)
0013-4651/2017/164(9)/X18/1/$37.00 © The Electrochemical Society

Erratum: Printing 3D Gel Polymer Electrolyte in Lithium-Ion Microbattery Using Stereolithography [*J. Electrochem. Soc.*, 164, A1852 (2017)]

Qiming Chen, Rong Xu, Zitao He, Kejie Zhao, and Liang Pan

School of Mechanical Engineering, Birck Nanotechnology Center, Purdue University, West Lafayette, Indiana 47906, USA

The article should include the following section:

Acknowledgments

Support for this work was provided by the National Science Foundation (NSF) (grant No. CMMI-1554189 and grant No. CMMI-1634832).